

# REACTION MECHANISM REQUIREMENTS IN SHOCK-INDUCED COMBUSTION SIMULATIONS

J. Keith Clutter, David W. Mikolaitis and Wei Shyy

Department of Aerospace Engineering, Mechanics & Engineering Science

University of Florida, Gainesville, Florida 32611.

Proceedings of the Combustion Institute, Vol. 28, (2000) pp.663-669, Twenty-Eighth  
International Symposium on Combustion, Edinburgh, Scotland, July 30 – August 4<sup>th</sup>.

28<sup>th</sup> International Combustion Symposium

Colloquium name: Detonations, Propellants, and Supersonic Combustion

Word count: 5103

Presentation choice: Oral

## **Abstract**

A quasi steady-state, shock-induced combustion problem due to the Mach 6.46 flight of a blunt projectile in a stoichiometric hydrogen and air mixture is examined as a case study. Three regions are identified where different elements of the chemical kinetics play key roles. The nose region is where the mixture is subjected to a near normal shock; the front separation region where the shock and reaction front diverge; and the separated front region in the far field where there is an oblique shock and a density front. These regions are at widely disparate temperatures and pressures. The near field is found to depend strongly on rate of heat release while the front separation point depends only on equilibrium, and the far field results depend strongly on a very accurate determination of the second explosion limit. Results also suggest factors which impact induction time, such as high-pressure effects in the reaction mechanisms, can play an important role.

## Introduction

Shock-induced combustion is relevant to many engineering problems in the areas of propulsion[1], munitions[2], and safety[3]. This combustion scenario also offers a kinetics modeling challenge because of the enormous range of temperatures and pressures encountered in the flow. While great progress in numerical algorithm development has been made in computation with detailed chemistry, there has been very little work in assessing the validity of reaction models over the range of conditions found in shock-induced combustion. Here the role of the chemical reaction mechanism in determining the flow field is studied in the context of a steady-state, shock-induced combustion problem. Information from the experimental investigation by Lehr[4], shown in Fig. 1, is used. The experiments entailed shooting projectiles at  $M=6.46$  into a stoichiometric mixture of hydrogen and air at a temperature of 293 K and a pressure of 320 Torr. Steady and unsteady combustion cases studied by Lehr have been used in several computational studies[5-16] in which the primary focus has been the development of numerical algorithms and various numerical treatments for the solution of the governing equations. A detailed review of these earlier studies is provided in [2]. In the present work the quasi steady-state case with  $M=6.46$  is the focus mostly because the resulting flow is relatively simple geometrically and key flow features are easily identified, but the enormous variation in pressure and temperature places heavy demands on the fidelity of the reaction model.

Figure 1 shows a shadowgraph from Lehr[4] with two distinct fronts that merge together near the front of the projectile. Similar results have been obtained by Kaneshige and Shepherd [17]. Keeping with the terminology of earlier studies, here the second front is labeled the reaction front. It is clearly a contour denoting a sharp change in density but the accuracy of this nomenclature will be revisited in the context of the current results. That the first is a shock is without question, but it is unclear from this image only whether or not the second front is a reaction front or a material surface separating burned from unburned gases. Indeed, it may be a reacting front near the shock and a material surface in the far field. In addition, the mechanism for front separation is not apparent from the shadowgraph. Here we will look closely at the nose region, front separation region, and far field to determine the most important features that a kinetic model must capture in order to successfully model the behavior in each region.

### **Kinetic Requirements in the Nose Region**

It is anticipated that stabilization of the detonation wave standing off the front of the projectile, as in this case, requires that the detonation wave be overdriven to a sufficiently high level. Calculation of the Chapman-Jouguet (CJ) Mach number for this case is a straightforward exercise, using W. C. Reynolds' Stanjan code for instance, yielding a CJ Mach number of approximately 5.0. This code is freely available [18]. The detonation wave in the nose region is now clearly shown to be overdriven and hence the flow behind the shock front along the stagnation streamline will not be expanded to sonic conditions by the chemical reaction behind the shock. Since the flowfield is fully subsonic between the shock front and the projectile, information about the pressure and

density field in the reaction zone will be felt throughout the nose region. Because of this the details of the heat release (rate of heat release or induction time, for example) will play key roles in determining the stand-off and overall shape of the detonation wave. Taking the mixture to be 55.6% N<sub>2</sub>, 29.6% H<sub>2</sub>, and 14.8% O<sub>2</sub>, the conditions behind the leading normal shock as approximately 2650 K and 20.4 atm. At such high temperatures it would be expected that HO<sub>2</sub>/H<sub>2</sub>O<sub>2</sub> chemistry would be relatively unimportant and that the important kinetics would be given solely by the main chain branching mechanism and recombination reactions.

This hypothesis can be tested very easily. Consider the mechanism drawn from GRI-Mech 2.11 [19] shown in Table 1. A similar mechanism has been used by Peterson, et al to investigate ignition delay in shock tubes [20]. Here we have run a constant volume explosion calculation using both the mechanism in Table 1 and the same mechanism with chain breaking reactions 6, 7, 8, and 9 removed. A plot of H<sub>2</sub>O formation as a function of time in Fig. 2 shows very little difference between the two cases. Therefore it seems likely that the feature of the chemical kinetics that must be modeled accurately at the high temperatures and pressures in the nose region are the main chain branching steps and the recombination steps involving O, OH, and H. It is entirely possible that a simple chemical model that does not include HO<sub>2</sub> and H<sub>2</sub>O<sub>2</sub> may work very well in this region and give good predictions of stand-off. Because of the high pressures, equilibrium temperatures in excess of 3300 K may be encountered. Reaction mechanisms that have been optimized for lower pressure and temperature reaction may be at a disadvantage when used in this region.

## **Kinetic Requirements in the Wave Separation Region**

Two possibilities immediately present themselves for why the waves separate. First, as the wave increases its inclination to the flow the Mach number of the normal velocity component falls. If it falls below the Chapman-Jouguet value then the wave can no longer remain as a steady detonation wave and presumably the reaction front would separate from the shock front. Another possibility is that as the Mach number of the normal velocity component falls the conditions behind the shock cross the second explosion limit and reaction effectively ceases. Calculations using Stanjan give a Chapman-Jouguet detonation Mach number slightly less than 5 for this mixture ( $M_{CJ} = 4.96$ ). The Mach number of the velocity component normal to the wave reaches this value at a wave angle of approximately  $50^\circ$ . Conditions behind a shock at this wave angle give a pressure and temperature of 1670 K and 12 atm which would place the conditions on the rapid reaction side of the second explosion limit and hence make the mixture rapidly reactive. This is to be expected, of course, since the mixture is within the detonation limits. If reaching the Chapman-Jouguet condition is the real reason for the wave separation, then the wave angle at separation will be insensitive to the details of the reaction mechanism and depend only on an accurate calculation of chemical equilibrium and the wave angle at the front separation point will be near  $50^\circ$  no matter how poor the kinetic model. Indeed, calculations of this flowfield using numerous different kinetic models all show the fronts separating at approximately the same wave angle [2]. The position in space where the waves separate will depend on the details of the subsonic nose region, however, and that calculation requires a good model for the high

pressure/high temperature region behind the normal shock. We will revisit the point about reaching the CJ point as the reason for the front separation in the next section.

### **Kinetic Requirements in the Far Field**

In the far field, as least as far as is visible in the shadowgraph of Lehr in Fig. 1, the shock wave is inclined at approximately  $26^\circ$  to the flow. The Mach number of the incident flow normal to the shock wave is therefore  $M=2.83$  corresponding a pressure of 1.96 atm and a temperature of 503 K behind the wave. Such an oblique shock will turn the flow about  $16^\circ$ , which is close to the angle of the second front. This indicates that in the far field one would expect that reaction is negligible and that the second front is not a reaction front, but merely a contact surface separating gases that had burned much earlier to those that were not burned. The results of a constant volume explosion calculation using the same subset of GRI-Mech 2.1 used before and starting at the conditions behind the far field shock and 55.6%  $N_2$ , 29.6%  $H_2$ , and 14.8%  $O_2$  shows virtually no reaction for times up to 100 seconds. The conjecture that the change in density front in the far field is a material surface is consistent with the calculation.

Assuming for the moment that the conjecture that the wave separation point is the CJ point, then in the vicinity of the wave separation point the second front is reacting and propagating, but is no longer tied directly to the shock. This can be verified by computing the reaction rates just behind the shock at the separation point. Taking the conditions behind the shock as 1670 K and 12 atm with 55.6%  $N_2$ , 29.6%  $H_2$ , and 14.8%

$O_2$ , the resulting constant volume explosion problem calculation is shown in Fig. 3. The reaction times are clearly within the fluid mechanical time scales of this problem.

Given that there is strong burning on the second front near the separation point and yet there is little to no reaction in the far field, one must explain why there should be a thin region separating the burned gases from the unburned. If the slowing down in rate of reaction is gradual along the front then there would be a thick, broadening transition from burned to unburned instead of the abrupt change seen in the shadowgraph. This implies that the transition from reacting to non-reacting must take place over a relatively narrow region. This can be explained in the context of the competition between the branching reaction  $H + O_2 \rightarrow OH + O$  and the chain breaking reaction  $H + O_2 + M \rightarrow HO_2 + M$ , i.e. the second explosion limit and its extrapolation.

As the now separated shock wave continues to turn and weaken, the temperature and pressure behind the shock continue to fall and may eventually cross the extrapolation second explosion limit. Material that crosses the shock outside of this point will react very slowly and may for practical purposes may be considered as non-reacting. Determination of this locus will depend on an accurate determination of the second explosion limit criterion.

Here we will look at a simple model with competing branching mechanisms to show the sensitivity of the rate in the vicinity of the crossover temperature.

Consider a simplified mechanism of the form



where  $A$  denotes reactants,  $X$  denotes nominally reactive intermediates, and  $Y$  denotes a less reactive intermediate, i.e the rate of  $A + Y \rightarrow X + X + X$  is much slower than the rate of  $A + X \rightarrow X + X + X$ . If  $k_1$ ,  $k_2$  and  $k_3$  are the rates of the three reactions and we linearize around an initial condition with finite  $A$ , the largest eigenvalue of the resulting linear system is

$$\lambda = \frac{-(k_3 - 2 \cdot k_1 + k_2) + \sqrt{(k_3 - 2 \cdot k_1 + k_2)^2 + 8 \cdot k_3 \cdot (k_1 + k_2)}}{2}. \quad (2)$$

If  $k_2 \rightarrow 0$  and  $k_3 \rightarrow 0$  with fixed  $k_1$ , then  $\lambda \rightarrow k_1$  which is the growth rate for uninhibited chain branching by the primary mechanism. If  $k_3 \rightarrow 0$  with  $k_1$  and  $k_2$  fixed, then  $\lambda \rightarrow k_1 - k_2/2$  which is the growth rate if  $Y$  denotes a chain terminator.

Now consider the case where  $k_3$  and  $k_1 - k_2/2$  are small compared to  $k_1$  corresponding to slow branching from the third reaction compared to the first and conditions close to the transition from one branching mechanism dominating the other.

Defining  $\varepsilon = k_3/(2 \cdot k_1)$  and  $\delta = (k_1 - k_2/2)/k_1$  it is readily determined that

$\delta \sim O(\varepsilon^{1/2})$  which motivates the choice of variable  $\delta = \eta \cdot \varepsilon^{1/2}$ . The asymptotic form for  $\lambda$  for  $\varepsilon \ll 1$  is

$$\lambda/k_1 \approx (\eta + \sqrt{\eta^2 + 12}) \cdot \varepsilon^{1/2}. \quad (3)$$

The important point is the reaction goes from fast to slow as the parameter  $\delta$  is varied over a range of  $\varepsilon^{1/2}$ , which is quite narrow. Since this factor is given by a difference, small errors in either term can give rise to a large relative error in  $\lambda$ , i.e. shift the reaction from the rapidly reactive to the weakly reactive region or vice versa. A representative plot with finite  $k_3$  ( $k_3 = 0.001$ ,  $k_1 = 1$ ) is shown in Fig. 4.

Now let's look at a case where the shock wave is inclined at  $45^\circ$  to the flow. This is beyond the CJ point and before the far field. Here the temperature behind the shock is approximately 886 K and the pressure is 5.218 atm. Once again we will start with 55.6%  $N_2$ , 29.6%  $H_2$ , and 14.8%  $O_2$ . The results of such a calculation are shown in Fig. 5. Here at time  $t=0$  the reaction is on the chain breaking side of the extrapolation of the second explosion limit and the slow branching rate is due to mechanisms involving  $HO_2$  and  $H_2O_2$ . As reaction proceeds, eventually the second explosion limit is crossed and after that reaction proceeds much more rapidly. Small changes in the branching or breaking rate will shift the second explosion limit condition which can move the crossover point a great distance in time.

Any expansion caused by reaction along the second front can be transmitted to the shock along Mach lines and help curve the shock. Therefore details about the rate of reaction along the second front from the CJ point to the second explosion limit point are important in determining the curvature of the shock as the shock moves away from the body. Accurate prediction of this part of the flow field will require accurate chemical kinetics for relatively cool temperatures (up to approximately 1700 K) and relatively low pressures (up to approximately 5 atm) and especially accurate capturing of the kinetics in the neighborhood of the second explosion limit. Because of the need for extreme

accuracy, it may be required to include small effects such as high pressure fall-off in order to get accurate enough kinetic rates.

### **Concluding Remarks**

Requirements on a kinetic scheme for predicting the  $M = 6.46$  shock initiation experiment of Lehr must be reasonably accurate in predicting the main branching and recombination reactions in the nose region where there are very high pressures in excess of 20 atm and temperatures over 3000 K. In the region where the fronts separate the mechanism need only predict any reasonably fast rate and correct equilibrium conditions and virtually any mechanism will do an adequate job. After the fronts have separated the mechanism must be able to give very accurate rate information for both the main branching mechanism and  $\text{HO}_2/\text{H}_2\text{O}_2$  chemistry so that the difference between the rates is computed with reasonable accuracy. A small error here will be magnified by differences of like numbers in computing the overall rate. Small errors here in the reaction rates can give rise to enormous differences in ignition times and hence give improper predictions for the curved shock region beyond the separation point. Numerical calculations with various kinetic schemes are in agreement with this point of view [2] and this topic will be the subject of a forthcoming paper.

Here we have shown evidence that the mechanism for the front splitting in the  $M=6.46$  shock initiation experiment of Lehr is due to the Mach number of the velocity

component normal to the shock falls below the Champan-Jouguet value so that a steady detonation front is no longer possible further away from the body.

Furthermore we have also demonstrated that in the far field the second front is not a reaction wave, but rather a material surface separating burned from unburned gases. Near the separation point the second front is a reacting wave. The reason why the front remains thin all the way from the separation point to the far field is that reaction is turned off quickly as conditions behind the shock cross the extrapolation of the second explosion limit curve.

### References

1. Rubins, P.M., and Bauer, R.C., *Journal of Propulsion and Power* 10:593-601 (1994).
2. Clutter, J.K., Mikolaitis, D.W. and Shyy, W., "Effect of Reaction Mechanism in Shock-Induced Combustion Simulations," AIAA Paper 98-0274, AIAA 36th Aerospace Sciences Meeting & Exhibit (1998).
3. Clutter, J.K. and Shyy, W., *Numerical Heat Transfer; Part B* 34:165-189 (1998).
4. Lehr, H.F., *Astronautica Acta* 17:589-597 (1972).
5. Yungster, S., Eberhardt, S. and Bruckner, A.P., *AIAA Journal* 29:187-199 (1991).
6. Lee, S. and Deiwert, G.S., "Calculation of Nonequilibrium Hydrogen-Air Reactions with Implicit Flux Vector Splitting Method," AIAA Paper 89-1700, AIAA, 24th Thermophysics Conference, Buffalo, NY (1989).
7. Wilson, G.J. and MacCormack, R.W., *AIAA Journal* 30:1008-1015 (1992).
8. Ahuja, J.K. and Tiwari, S.N., "Numerical Simulation of Shock-Induced Combustion in a Superdetonative Hydrogen-Air System," AIAA Paper 93-0242, AIAA, 31st Aerospace Sciences Meeting, Reno, NV (1993).
9. Sussman, M.A., "Source Term Evaluation for Combustion Modeling," AIAA Paper 93-0239, AIAA, 31st Aerospace Sciences Meeting, Reno (1993).

10. Wilson, G.J. and Sussman, M.A., *AIAA Journal* 31:294-301 (1993).
11. Shang, H.M., Chen, Y.S., Liaw, P., Chen, C.P. and Wang, T.S., "Investigation of Chemical Kinetics Integration Algorithms for Reacting Flows," AIAA Paper 95-0806, AIAA, 33rd Aerospace Sciences Meeting, Reno, NV (1995).
12. Matsuo, A., Fujii, K. and Fujiwara, T., *AIAA Journal* 33:1056-1063 (1995).
13. Matsuo, A. and Fujiwara, T., *AIAA Journal* 31:1835-1841 (1993).
14. Sussman, M.A., "A Computational Study of Unsteady Shock-Induced Combustion of Hydrogen-Air Mixtures," AIAA Paper 94-3101, AIAA, 18th Aerospace Ground Testing Conference, Colorado Springs, CO (1994).
15. Matsuo, A. and Fujii, K., *AIAA Journal* 33:1828-1836 (1995).
16. Matsuo, A. and Fujii, K., "First Damk<sup>1/2</sup>hler Parameter for Prediction and Classification of Unsteady Combustions Around Hypersonic Projectiles," AIAA Paper 96-3137, AIAA/ASME/SAE/ASEE, 32nd Joint Propulsion Conference, Lake Buena Vista, FL (1996).
17. M. J. Kaneshige, and J. E. Shepherd, *Proc. Combust. Inst.* 26:3015-3022 (1996).
18. PC-Chemkin, V3.8 of the interpreter, 4.9 of the library, and 3.1 of the transport library. Available from <http://www.galcit.caltech.edu/EDL/public/codes.html> courtesy of Joseph Shepherd.
19. C.T. Bowman, R.K. Hanson, D.F. Davidson, W.C. Gardiner, Jr., V. Lissianski, G.P. Smith, D.M. Golden, M. Frenklach and M. Goldenberg, [http://www.me.berkeley.edu/gri\\_mech/](http://www.me.berkeley.edu/gri_mech/).
20. Petersen, E. L., Davidson, D. F., Röhrig, M., and Hanson, R. K., Proceedings of the 20th International Symposium on Shock Waves, v. II, (B. Sturtevant, J. E. Shepherd, and H. G. Hornung, Eds.), World Scientific, Singapore, 1995, p. 941.

**Table 1. Hydrogen-Air mechanism from GRI-Mech 2.11 (Units are moles, cubic centimeters, seconds, Kelvin, and calories/mole).**

	REACTION <sup>a</sup>	A	n	E
1	2O+M = O2+M H2/ 2.40/ H2O/15.40/	1.20E+17	-1	0
2	O+H+M = OH+M H2/2.00/ H2O/6.00/	5.00E+17	-1	0
3	O+H2 = H+OH	5.00E+04	2.67	6290
4	O+HO2 = OH+O2	2.00E+13	0	0
5	O+H2O2 = OH+HO2	9.63E+06	2	4000
6	H+O2+M = HO2+M O2/ .00/ H2O/ .00/ N2/ .00/	2.80E+18	-0.86	0
7	H+2O2 = HO2+O2	3.00E+20	-1.72	0
8	H+O2+N2 = HO2+N2	3.75E+20	-1.72	0
9	H+O2+H2O = HO2+H2O	9.38E+18	-0.76	0
10	H+O2 = O+OH	8.30E+13	0	14413
11	2H+M = H2+M H2/ .00/ H2O/ .00/	1.00E+18	-1	0
12	2H+H2 = 2H2	9.00E+16	-0.6	0
13	2H+H2O → H2+H2O	6.00E+19	-1.25	0
14	H+OH+M = H2O+M H2/ .73/ H2O/3.65/	2.20E+22	-2	0
15	H+HO2 = O+H2O	3.97E+12	0	671
16	H+HO2 = O2+H2	2.80E+13	0	1068
17	H+HO2 = 2OH	1.34E+14	0	635
18	H+H2O2 = HO2+H2	1.21E+07	2	5200
19	H+H2O2 = OH+H2O	1.00E+13	0	3600
20	OH+H2 = H+H2O	2.16E+08	1.51	3430
21	2OH(+M) = H2O2(+M) High Pressure Limit <sup>b</sup> 2OH+M = H2O2+M Low Pressure Limit H2/2.00/ H2O/6.00/	7.40E+13 2.30E+18	-0.37 -0.900	0 -1700
22	2OH = O+H2O	3.57E+04	2.4	-2110
23	OH+HO2 = O2+H2O	2.90E+13	0	-500
24	OH+H2O2 = HO2+H2O	1.75E+12	0	320
25	OH+H2O2 = HO2+H2O	5.80E+14	0	9560
26	2HO2 = O2+H2O2	1.30E+11	0	-1630
27	2HO2 = O2+H2O2	4.20E+14	0	12000
28	N+NO = N2+O	3.50E+13	0	330
29	N+O2 = NO+O	2.65E+12	0	6400
30	N+OH = NO+H	7.33E+13	0	1120
31	N2O+O = N2+O2	1.40E+12	0	10810
32	N2O+O = 2NO	2.90E+13	0	23150
33	N2O+H = N2+OH	4.40E+14	0	18880
34	N2O+OH = N2+HO2	2.00E+12	0	21060
35	N2O(+M) = N2+O(+M) High pressure limit <sup>c</sup> N2O+M = N2+O+M Low pressure limit H2/2.00/ H2O/6.00/	1.30E+11 6.20E+14	0 0	59620 56100

36	HO <sub>2</sub> +NO = NO <sub>2</sub> +OH	2.11E+12	0	-480
37	NO+O+M = NO <sub>2</sub> +M H <sub>2</sub> /2.00/ H <sub>2</sub> O/6.00/	1.06E+20	-1.41	0
38	NO <sub>2</sub> +O = NO+O <sub>2</sub>	3.90E+12	0	-240
39	NO <sub>2</sub> +H = NO+OH	1.32E+14	0	360
40	NH+O = NO+H	5.00E+13	0	0
41	NH+H = N+H <sub>2</sub>	3.20E+13	0	330
42	NH+OH = HNO+H	2.00E+13	0	0
43	NH+OH = N+H <sub>2</sub> O	2.00E+09	1.2	0
44	NH+O <sub>2</sub> = HNO+O	4.61E+05	2	6500
45	NH+O <sub>2</sub> = NO+OH	1.28E+06	1.5	100
46	NH+N = N <sub>2</sub> +H	1.50E+13	0	0
47	NH+H <sub>2</sub> O = HNO+H <sub>2</sub>	2.00E+13	0	13850
48	NH+NO = N <sub>2</sub> +OH	2.16E+13	-0.23	0
49	NH+NO = N <sub>2</sub> O+H	4.16E+14	-0.45	0
50	NH <sub>2</sub> +O = OH+NH	7.00E+12	0	0
51	NH <sub>2</sub> +O = H+HNO	4.60E+13	0	0
52	NH <sub>2</sub> +H = NH+H <sub>2</sub>	4.00E+13	0	3650
53	NH <sub>2</sub> +OH = NH+H <sub>2</sub> O	9.00E+07	1.5	-460
54	NNH = N <sub>2</sub> +H	3.30E+08	0	0
55	NNH+M = N <sub>2</sub> +H+M H <sub>2</sub> /2.00/ H <sub>2</sub> O/6.00/	1.30E+14	-0.11	4980
56	NNH+O <sub>2</sub> = HO <sub>2</sub> +N <sub>2</sub>	5.00E+12	0	0
57	NNH+O = OH+N <sub>2</sub>	2.50E+13	0	0
58	NNH+O = NH+NO	7.00E+13	0	0
59	NNH+H = H <sub>2</sub> +N <sub>2</sub>	5.00E+13	0	0
60	NNH+OH = H <sub>2</sub> O+N <sub>2</sub>	2.00E+13	0	0
61	H+NO+M = HNO+M H <sub>2</sub> /2.00/ H <sub>2</sub> O/6.00/	8.95E+19	-1.32	740
62	HNO+O = NO+OH	2.50E+13	0	0
63	HNO+H = H <sub>2</sub> +NO	4.50E+11	0.72	660
64	HNO+OH = NO+H <sub>2</sub> O	1.30E+07	1.9	-950
65	HNO+O <sub>2</sub> = HO <sub>2</sub> +NO	1.00E+13	0	13000
66	NH <sub>3</sub> +H = NH <sub>2</sub> +H <sub>2</sub>	5.40E+05	2.4	9915
67	NH <sub>3</sub> +OH = NH <sub>2</sub> +H <sub>2</sub> O	5.00E+07	1.6	955
68	NH <sub>3</sub> +O = NH <sub>2</sub> +OH	9.40E+06	1.94	6460

<sup>a</sup>Third body efficiencies for reactions 1, 2, 6, 11, 14, 21, 35, 37, 55, and 61 are relative to argon.

<sup>b</sup>Rate given by the Troe form where  $k = k_{\infty} \cdot \left( \frac{P_r}{1 + P_r} \right)$ ,  $P_r = \frac{k_o \cdot [M]}{k_{\infty}}$ ,

$$\log(F) = \left\{ 1 + \left[ \frac{\log(P_r) + c}{n - d \cdot (\log(P_r) + c)} \right]^2 \right\}^{-1} \cdot \log(F_c),$$

$c = -0.4 - 0.67 \cdot \log(F_c)$ ,  $n = 0.75 - 1.27 \cdot \log(F_c)$ ,  $d = 0.14$ , and

$$F_c = (1 - .7346) \cdot \exp(-T/94 K) + .7346 \cdot \exp(-T/1756 K) + \exp(-5182 K/T).$$

<sup>c</sup>Rate given by the Lindeman form:  $k = k_0 k_{\infty} [M] / (k_{\infty} + k_0 [M])$  where  $k_0$  is the low pressure limit expression and  $k_{\infty}$  is the high pressure limit expression.

## Figure Captions

Figure 1. Shadowgraph for M=6.46 projectile from Lehr[4].

Figure 2. Reaction in the nose region of the projectile.

Figure 3. Constant volume explosion calculation for conditions near the CJ point.

Figure 4. Growth rate versus termination rate.

Figure 5. Constant volume explosion results for conditions behind the shock inclined at 45 ° to the flow.

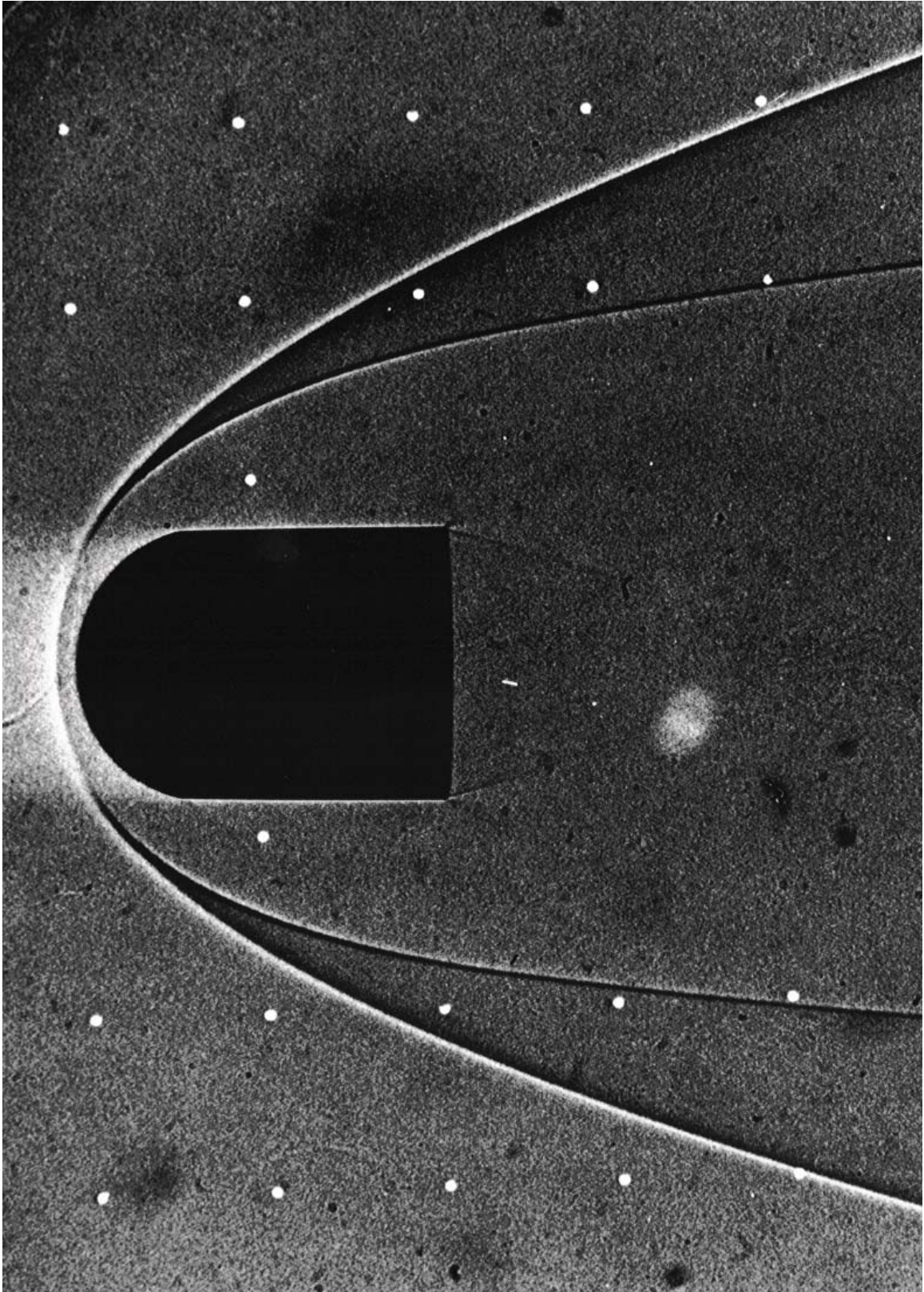


Figure 1

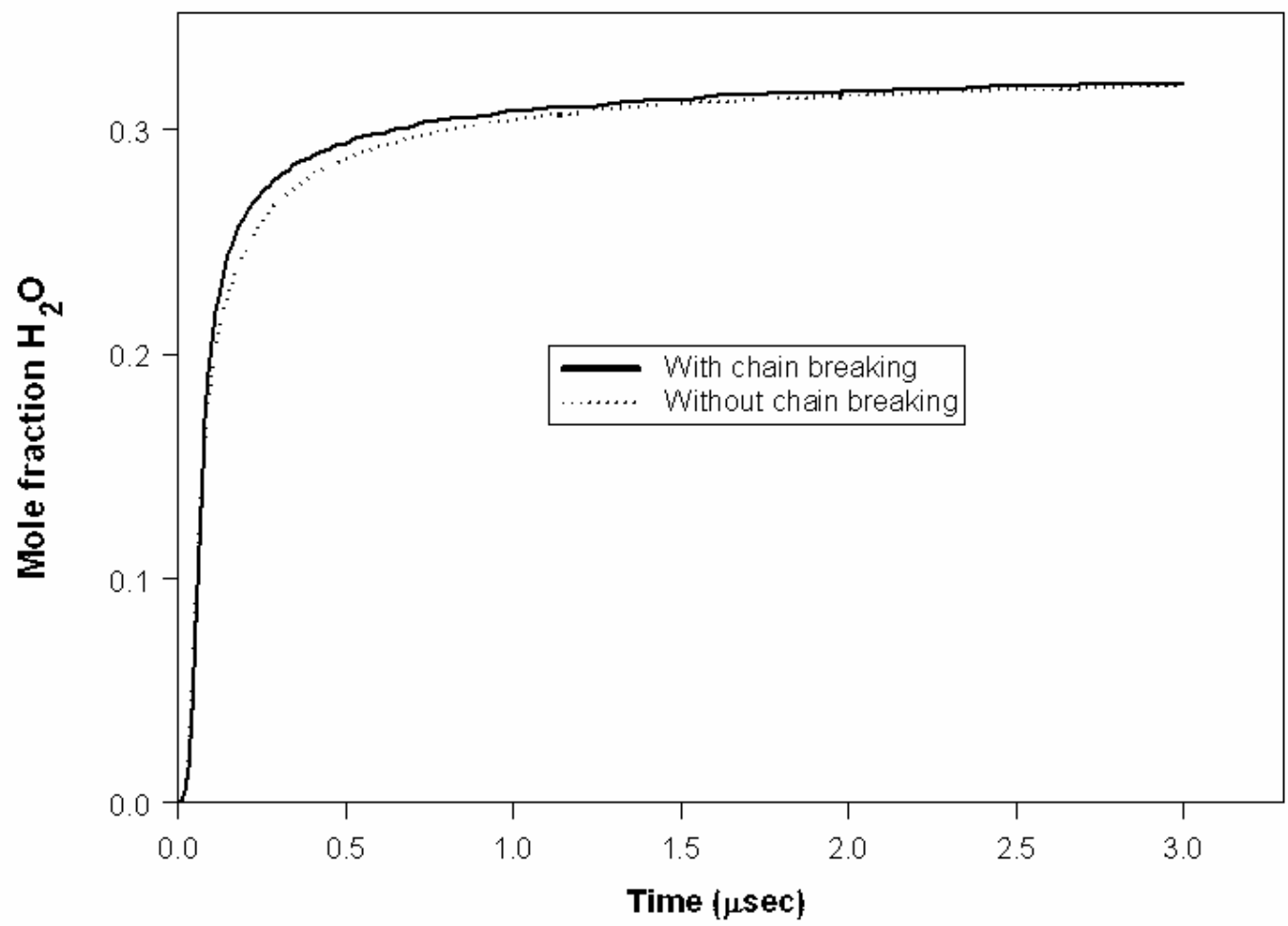


Figure 2

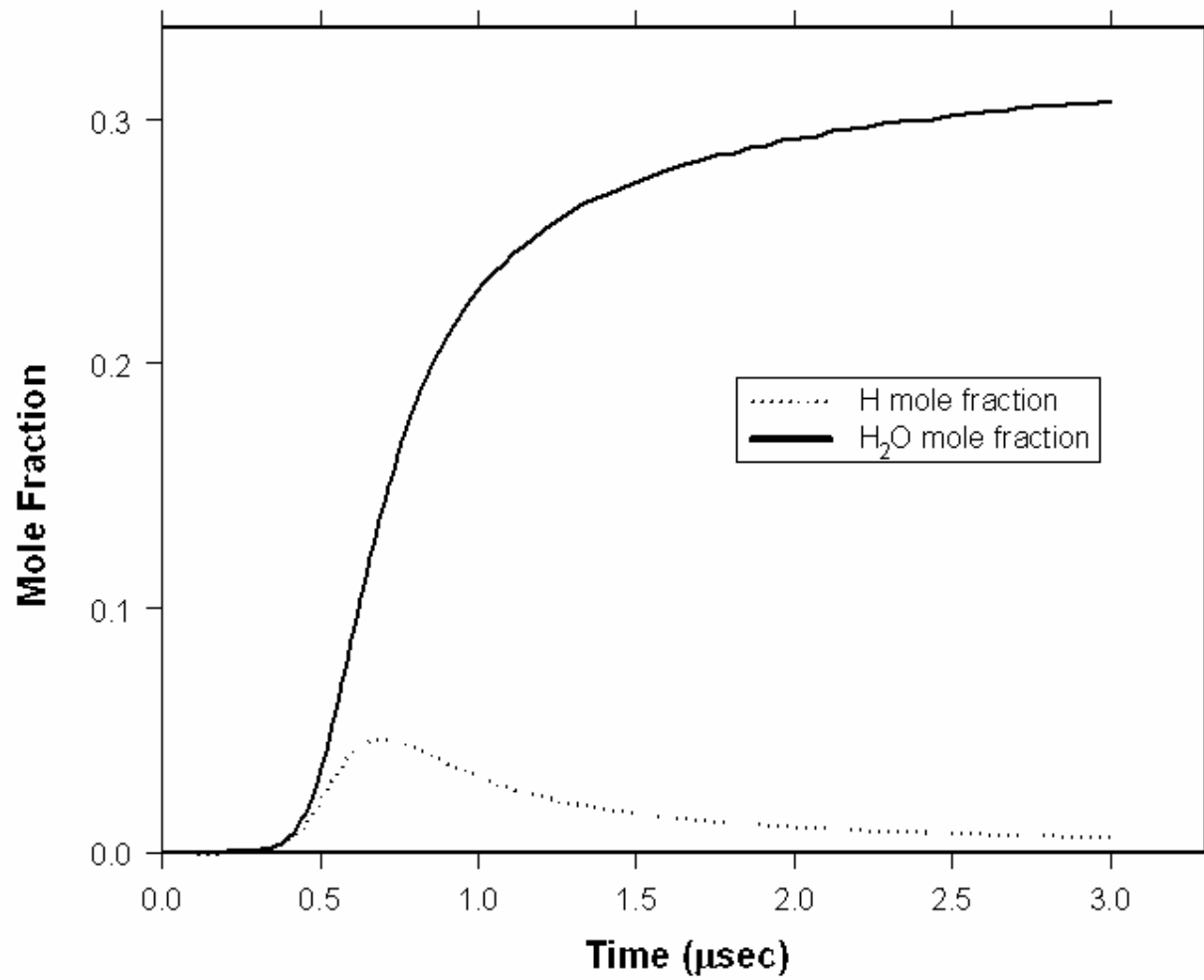


Figure 3

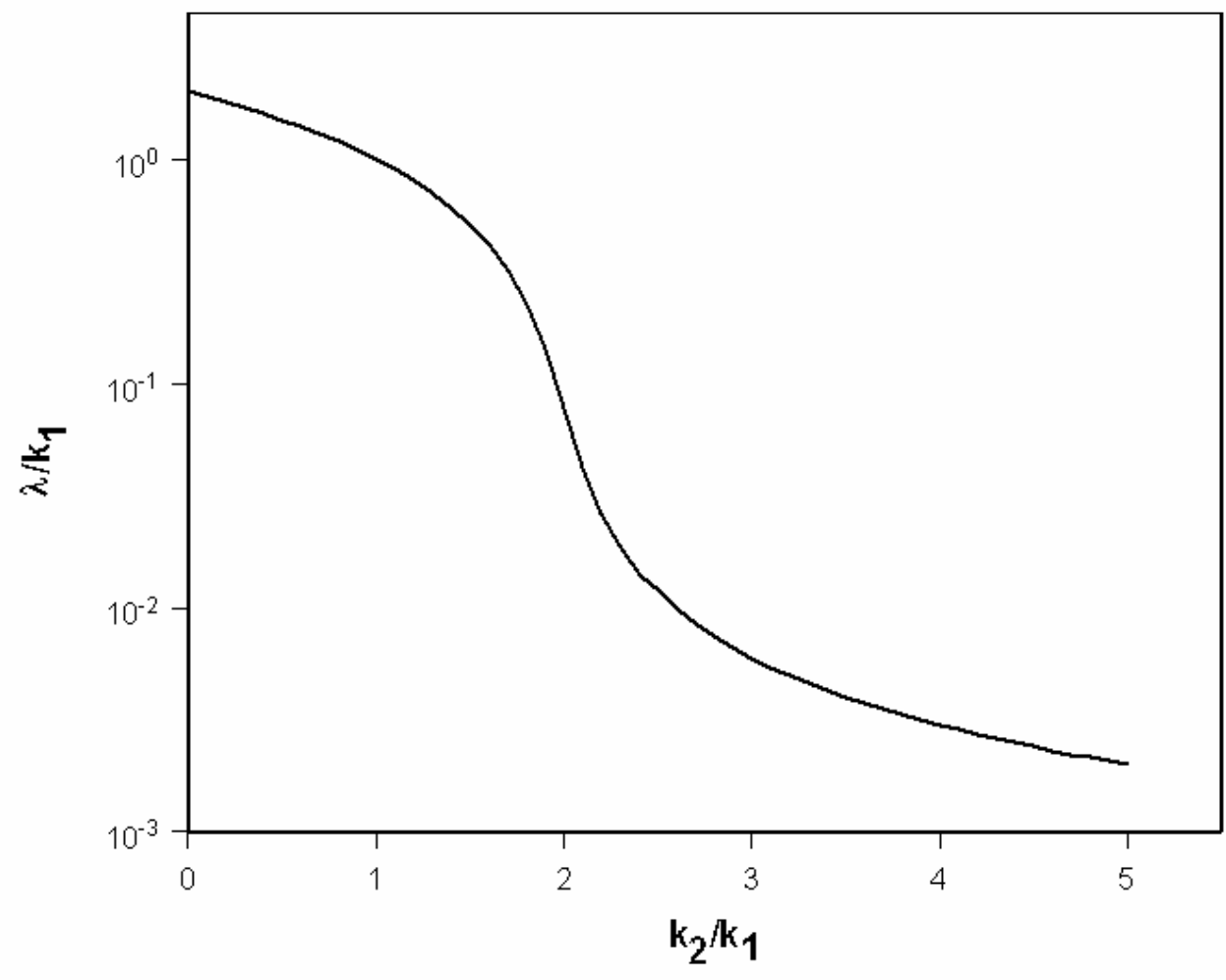


Figure 4

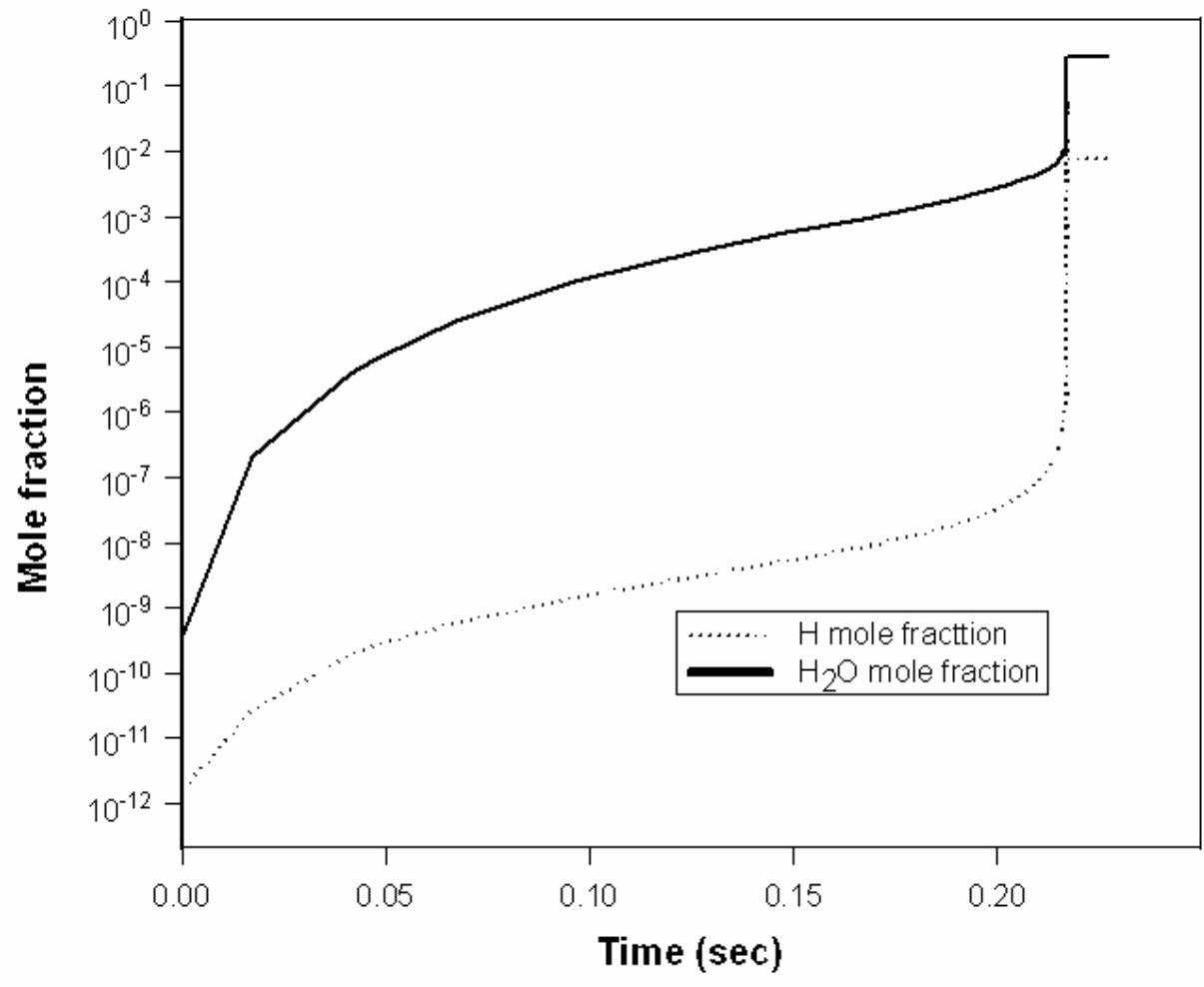


Figure 5